Materials Science Forum Vols. 600-603 (2009) pp 267-272
online at http://www.scientific.net

Investigation of Defect Formation in 4H-SiC(0001) and (000-1) epitaxy

H. Tsuchida[1, a], I. Kamata[1,b] and M. Nagano[1,c]

[1]Central Research Institute of Electric Power Industry (CRIEPI)

2-6-1 Nagasaka, Yokosuka, Kanagawa 240-0196, Japan

[a]tsuchida@criepi.denken.or.jp, [b]kamata@criepi.denken.or.jp, [c]m-nagano@criepi.denken.or.jp

Keywords: epitaxy, dislocation, stacking fault, X-ray topography, TEM

Abstract. Defect formation in 4H-SiC(0001) and (000-1) epitaxy is investigated by grazing incidence synchrotron reflection X-ray topography and transmission electron microscopy. Frank-type faults, which are terminated by four Frank partials with a 1/4[0001] type Burgers vector with the same sign on four different basal planes, are confirmed to be formed by conversion of a 1*c* threading edge dislocation (TSD) in the substrate as well as simultaneous generation of a 1*c* TSD during epitaxy. The collation between the topography appearance and the microscopic structure and the variety of Frank faults are shown. Formation of carrot defects and threading dislocation clusters are also investigated.

Introduction

Enlargement of the device active area is a technological challenge in the development of high-power 4H-SiC devices, and reduction of extended defects in the epilayers is a key issue to obtain large active-area devices. Several types of defect propagation/conversion and nucleation near the epilayer/substrate interface have been reported [1-6], although the full picture remains unclear. In this paper, we investigate defect formation in 4H-SiC(0001) and (000-1) epitaxy by grazing incidence synchrotron reflection X-ray topography and transmission electron microscopy (TEM).

Experiment

Epitaxial growth was performed in a vertical hot-wall reactor [7] with a H_2+SiH_4+C_3H_8 system on commercial 4H-SiC(0001) and (000-1) substrates 8° off-cut towards <11-20>. The growth conditions were 1545°C and 42 Torr. Grazing incidence synchrotron reflection X-ray topography was performed with g=11-28 using a monochromatic beam (λ=1.541 Å) at SPring-8 BL16 [6]. The topography images were recorded on nuclear emulsion plates for the same wafers before and after the epitaxial growth, and defect propagation/convertion and generation were tracked. Cross-sectional TEM was performed with a electron beam along the [11-20] down-step direction.

Results and discussion

TSD-SF defects Figures 1(a) and 1(b) show X-ray topography images taken before and after 4H-SiC(0001) epitaxy. In a comparison of the images, a TSD marked A in the substrate is confirmed to be converted into a defect showing a linear contrast marked B. The defect propagates towards the down-step [11-20] direction. A pair of oval pits is found at the surface end position of the defect after KOH etching, indicating the presence of a stacking fault on the basal plane. Therefore we call this type of defect as a "TSD-SF converted defect" [6]. We note that no morphological disturbance is observed on the as-grown surface at the corresponding position of the defect.

Figure 2 shows cross-sectional TEM images taken from a stacking fault of a "TSD-SF converted defect". The position of the stacking fault was tracked by making collation between the topography image and KOH etched feature. Then a section including the stacking fault was cut off from the epilayer sample. The cross-sectional TEM image was taken through the down-step [11-20] direction.

The low-magnification cross-sectional TEM image shown in Fig. 2(a) confirms the presence of a stacking fault on the basal plane. The width of the stacking fault is confirmed to be ~1.4 μm along the [1-100] direction, which is perpendicular to the down-step direction. Figure 2(b) shows a high-resolution TEM image taken from the right edge, which is indicated as area-1 in Fig. 2(a), of the stacking fault. In Fig. 2(b), a Frank partial (FP1) creating a missing layer on the left side is found. The perfect 4H A'C'/AB/A'C'/AB/A'C'/AB (222222) stacking is converted into A'C'/ABCAB/A'C'/AB (2522) stacking at FP1 from the right to left. This (2522) stacking is expected from an intrinsic fault and confirms that the Frank partial FP1 has a 1/4[0001] type Burgers vector. Figure 2(c) shows a high-resolution TEM image taken from the left edge, which is indicated as area-2 in Fig. 2(a), of the stacking fault. In this area, three Frank partials FP2, FP3 and FP4 are found. All four Frank partials have the same sign that create a missing layer on the left side (or an extra layer on the right side), forming a series of faults. The four Frank partials are locating on four different basal planes. Only one side of the respective extra planes is terminated by one Frank partial and the other side is not terminated. These findings coincide perfectly with that expected from dissociation of a 1*c* TSD into four Frank partials having a 1/4[0001] type Burgers vector. In Fig. 2(c), from the right to left, A'C'/ABCAB/A'C'/AB (2522) stacking as that of a "single missing layer fault" converts into A'C'/ABCA/C'B'A'/B/ (2431) stacking by FP2 as that of a "double missing layers fault", followed by A'C'/ABCA/C'/AB/ (2412) stacking by FP3 as that of a "triple missing layers fault" and then returning to the perfect A'C'/AB/A'C'/AB (2222) 4H stacking. Each transition can also be termed a "single extra layer fault", "double extra layers fault" and "triple extra layers fault" from the left to right in Figs. 2(b) and 2(c). Formation of a pair of opposite sense 1/3<1-100> shifts is also suggested to explane the stacking change at around FP2. The (2522) stacking dominets the entire structure of the Frank fault in Fig. 2 more than 98% in width. The width ratio of each fault is evaluated to be 1 : 0.004 : 0.009 (single : double : triple missing layers). We note that the exact stacking sequences are different for another investigated Frank faults in the epilayer, whereas the width ratio remains a minor difference.

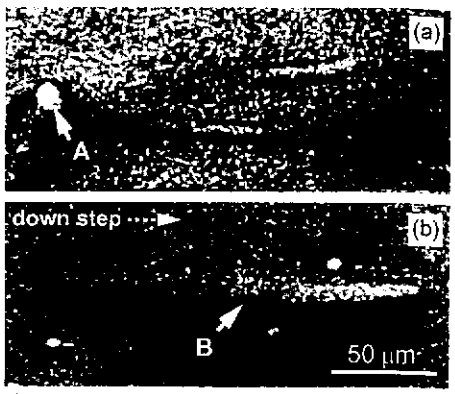

Fig. 1. X-ray topography images (g=11-28) taken (a) before (sustrate) and (b) after 4H-SiC (0001) epitaxy.

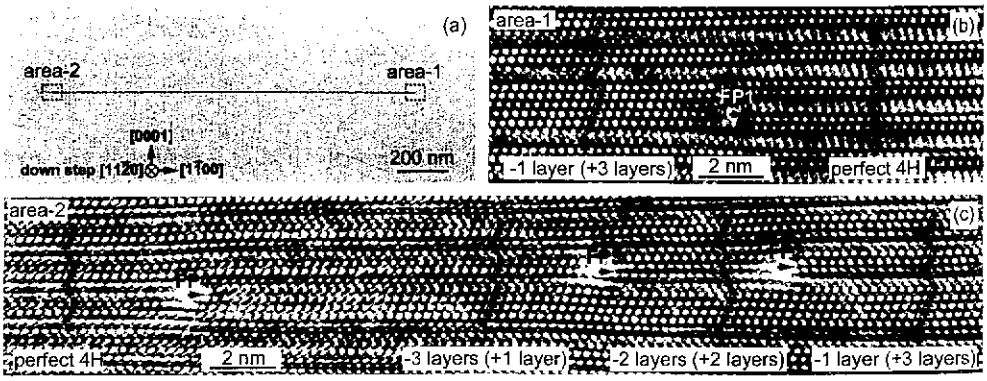

Fig. 2. (a) Low-magnification cross-sectional TEM image of a Frank fault of a "TSD-SF converted defect" and high-resolution TEM images taken for (b) area-1 (the right edge) and (c) area-2 (the left edge) of the fault. The images are taken through the down-step [11-20] direction.

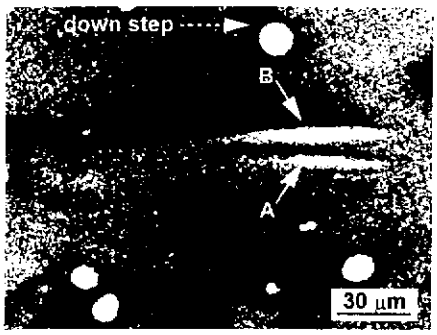

Fig. 3. X-ray topography image (g=11-28) taken for a Frank fault of a "TSD-SF converted defect".

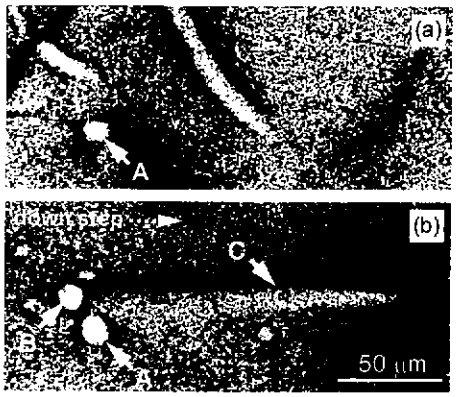

Fig. 4. X-ray topography images (g=11-28) taken (a) before (sustrate) and (b) after 4H-SiC (0001) epitaxy.

In Fig. 1(b), the topography contrast of the Frank fault is edged with a dark shadow on the right-side towards the down-step direction. On the other hand, we also find topography contrast of Frank faults edged with a dark shadow on the left side towards down-step with almost the same frequency [6]. The defect in Fig. 2, which has the Frank partials creating a missing layer on the left side towards the down-step direction, shows a dark shadow on the left side of the defect topography contrast. We have confirmed that the dark shadow on the topography contrast always corresponds to the missing layer side of the Frank partials. This suggests that the fine appearance of topography contrast reflects the microscopic structure of the defect, indicating the sign of the Frank partials.

Figure 3 shows a topography image of another Frank fault converted from a TSD in the substrate. The epilayer thickness is ~20 μm. The topography contrast of this particular Frank fault splits into two lines marked A and B at the middle section of the defect. The separation distance of the split contrast is ~13 μm near the surface end. The linear contrast marked A is thinner than that marked B, while both linear contrast show a dark shadow on the same side. Taking account into the defect microstructure shown in Fig. 2 and the collation between the dark shadow on the topography contrast and the sign of the Frank partials, the linear contrast marked A and B can correspond to one partial and the other three partials, respectively, leaving a single missing layer fault between them. In this case, the defect topography contrast is observed to split into two lines, since the separation distance between one partial and other three partials is sufficiently wide to distinguish them.

Figures 4(a) and 4(b) show X-ray topography images taken before and after 4H-SiC(0001) epitaxy. A TSD marked A in the substrate is confirmed to propagate as a TSD marked A'. This type of TSD propagation from the substrate into the epilayer dominates in the 4H-SiC epitaxy. On the other hand, a defect with circular bright contrast corresponding to a TSD marked B is confirmed to be newly generated during the epitaxial growth in areas where no dislocation is existing in the substrate. At the same time, thick linear contrast [marked C in Fig. 4(b)] propagating to the down-step direction is found to be generated during the epitaxy. No morphological disturbance is observed on the as-grown surface at the corresponding position of the linear defect contrast. The topography feature of the linear defect is exactly the same as that of "TSD-SF converted defects". Moreover, a closely arranged pair of oval KOH pits is confirmed at the surface end position of the defect [6]. These findings suggest that the same type of Frank faults on the basal plane can be formed by not only through conversion of a TSD in the substrate ("TSD-SF converted defects") but also simultaneous generation of a new TSD connecting with the fault during epitaxy. Therefore, we call this type of newly generated defect as a "TSD-SF nucleated defect" [6]. We have confirmed that the Frank fault of a "TSD-SF nucleated defects" also consists of four Frank partials having a 1/4[0001] type Burgers vector as same as that of the "TSD-SF converted defect" shown in Fig. 2 by high-resolution TEM.

The majority of the "TSD-SF converted defects" form as type-A in Fig. 5, while a small number (< 1 cm^2) re-convert to a TSD again as type-A' in Fig. 5 [topography image in Fig. 6(a)]. Meanwhile, the majority of "TSD-SF nucleated defects" form as type-B in Fig. 5, while a small number (< 1 cm^2) also form a pair of new TSDs connected by a Frank fault as type-B' in Fig. 5 [topography image in Fig. 6(b)]. As revealed by the collation between the topography image and the microscopic structure of the Frank faults, the Frank partials of both "TSD-SF converted defects" and "TSD-SF nucleated defects" can have one of the two signs, i.e. left side missing layer (right side extra layer) and right side missing layer (left side extra layer) towards the down-step direction. It can be expected that a left side missing layer (right side extra layer) Frank faults of a "TSD-SF converted defect" is originated from a right-handled TSD in the substrate, and a right side missing layer (left side extra layer) Frank faults is originated from a left-handled TSD. In the case of "TSD-SF nucleated defects", a pair of a right side missing layer (left side extra layer) Frank fault and a right-handled TSD and a pair of a left side missing layer (right side extra layer) Frank fault and a left-handled TSD can be nucleated simulteneously. As shown by type-A' in Fig. 5, the original TSD and the revived TSD should have the same sign if a TSD in the substrate converts once into a Frank fault and then converts again into a TSD. In the case of pair generation of TSDs connected by a Frank fault as type-B' in Fig. 5, the two TSDs should have opposite signs. We also confirmed that a small number (< 1 cm^2) of similar defects on the basal plane are formed by pair generation of opposite sign Frank partials as type-C in Fig. 5 [topography image in Fig. 6(c)] without any connection with a TSD. The pair generation of opposite sign Frank partials indicates that a Frank fault terminated by the frank partials at both sides on the same basal plane also exists in the epilayer.

Figure 7 shows the correlations between the density of TSDs in the substrates and the densities of "TSD-SF converted defects" and "TSD-SF nucleated defects". As expected from the connection with a TSD in the substrate, the density of "TSD-SF converted defects" proportionally increases with the density of TSDs in the substrates. The conversion ratio from a TSD to a "TSD-SF converted defect" is ~0.07 %. On the other hand, the density of "TSD-SF nucleated defects" also shows proportional

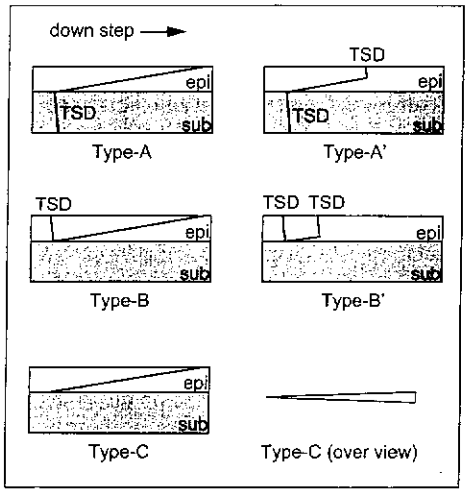

Fig. 5 Schematic models of the observed Frank fault formation by conversion of a TSD in the substrate (type-A, A'), simulatneous generation of a new TSD (type-B, B') and pair generation of opposite sign Frank partials.

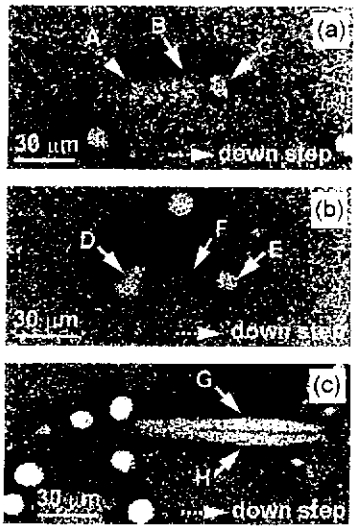

Fig. 6 Topography images (g=11-28) showing (a) TSD (marked A)→SF (marked B)→TSD (marked C) convertion, (b) pair generation of TSDs (marked D and E) via SF (marked F) and (c) pair generation of opposite sign Frank partials (marked G and H).

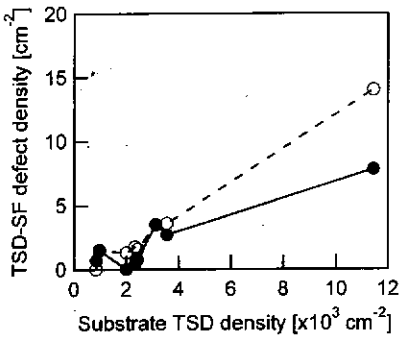

Fig. 7 Correlation between density of TSDs in the substrates and densities of "TSD-SF converted defects" (closed circles) and "TSD-SF nucleated defects" (open circles) in 4H-SiC{0001} epilayers.

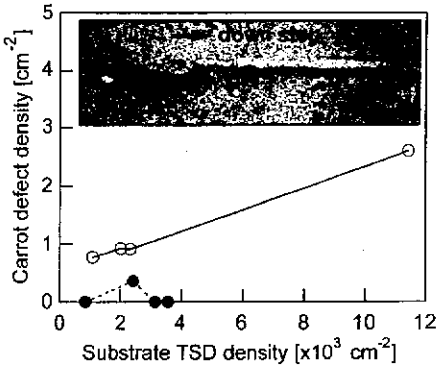

Fig. 8 Correlation between density of TSDs in the substrate and density of carrot defects [open circles: (0001)Si-face, closed circles: (000-1)C-face]. The inset shows a topography image of a carrot defect.

increase with the density of TSDs in the substrates. This suggests that both "TSD-SF converted defects" and "TSD-SF nucleated defects" involve a similar formation mechanism. Based on the evaluated microscopic structure of the Frank faults, we suggest that covering spiral-steps with off-steps is a possible cause for both types of Frank fault formation. We note that the stacking of 8H polytype inclusions [5] is completely different from that of the Frank faults of "TSD-SF converted defects" and "TSD-SF nucleated defects". The topography appearance of the 8H polytype inclusions, which shows no defect contrast in topography with g=11-28 and 1-108 [6], is also different completely from that of the Frank faults.

Carrot defects Carrot defects have been reported to consist of a Frank fault on the basal plane and a prismatic fault connected by a stair-rod dislocation [3]. It has been also reported that a TSD in the substrate is connected to the carrot defects. Figure 8 shows the correlation between the density of TSDs in the substrates and the density of carrot defects in 4H-SiC{0001} epilayers. The inset of Fig. 8 shows a typical topography image of a carrot defect. All the carrot defects in Fig. 8 were confirmed to be connected to a TSD in the substrates by a comparison of topography images taken before and after epitaxial growth [6]. In the comparison, we also confirmed the presence of a small number of defects (<<1 cm^{-2} in typical) showing "carrot-like" feature in as-grown morphology without any connection to a TSD in the substrate. Since this kind of "carrot-like" defect can involve a different formation mechanism, we did not include them in Fig. 8. As shown by the open circles in Fig. 8, the density of carrot defects for the 4H-SiC(0001) epilayers is confirmed to increase proportionaly with the density of TSDs in the substrates. This agrees with that the carrot defects connect to a TSD in the substrate. The convertion ratio from a TSD to a carrot defect is evaluated to be ~0.02%.

The density of carrot defects for the (000-1) epilayers is found to be significantly smaller than that for the (0001) epilayers as shown by the closed circles in Fig. 8. We supeculate that a difference in surface morphology as well as step structure around a TSD on the H_2-etched surface and grown surface can influence the convertion ratio from a TSD to a carrot defect. Possible interaction of a BPD with a TSD at the starting point of carrot defects was suspected because of the structure and Burgers vector of the defects [4, 6]. In our topography images, a BPD is observed to connect with a TSD at the starting point of some (not all) of the carrot defects [6]. Although it is still unclear if an interaction with a BPD and TSD can promote formation of carrot defects, a flatter surface on the H_2-etched surface and grown surface can minimize the chance of meeting a BPD and a TSD at the surface. This coincides with the smaller conversion ratio from a TSD to a carrot defect on the (000-1) epitaxy, since the (000-1) epitaxy tends to show a flatter surface. More study is crearly needed for the formation mechanism of carrot defects.

Threading dislocation clusters Figure 9 shows X-ray topography images taken (a) before and (b) after 4H-SiC epitaxial growth. Before taking the image Fig. 9(a), high-temperature H_2 etching at 1400°C was performed to the substrate. In a comparison with the topography images before and after epitaxial growth, the substrate defect consisting of an array of BPDs shown in Fig. 9(a) is confirmed to induce the array of TEDs in the epilayer shown in Fig. 9(b). In Fig. 9(a), the BPDs are confirmed to form in loops or half-loops. Formation of the array of TEDs in the epilayer can be understood by dislocation conversion from BPDs to TEDs during epitaxial growth [1]. We also confirmed by successive polishing and KOH etching analysis that the BPD loops shown in Fig. 9(a) are localized near the substrate surface. Since the arrays of BPD loops are localized near the surface, we interpret their origin to be related to the substrate preparation process including polishing and in-situ H_2 etching processes. As the common feature of this type of defect, we find a cluster or array of TEDs along the defect after KOH etching. We also find surface disturbance along the TED array on the as-grown surface [6]. The particular surface disturbance for the defect shown in Fig. 9(b) is rather linear and long with an entire length of ~750 μm almost perpendicular to the down-step direction, although we find similar defects of various shapes, direction and length/size (typically shorter than 100 μm). The density of this type of defect can vary from zero to several per cm^2. We note that small (or short) TED clusters showing no clear evidence of BPD loops in the topography images taken before epitaxial growth are also found with a density from less than 1 to 36 cm^{-2} with a average of 12 cm^{-2} in the investigated samples.

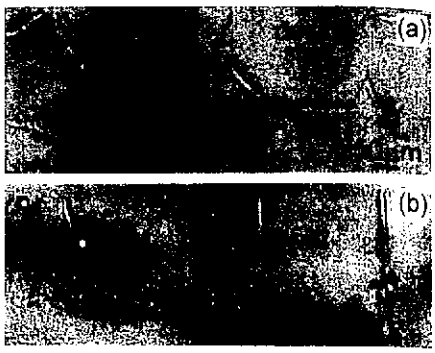

Fig. 9 X-ray topography images (g=11-28) taken (a) before and (b) after 4H-SiC(0001) epitaxy showing formation of a TED array.

Summary

Formation of Frank-type faults, which are terminated by four Frank partials with a 1/4[0001] type Burgers vector on four different basal planes, is confirmed by X-ray topography and TEM. The Frank faults are formed by conversion of a 1*c* TSD in the substrate as well as simultaneous generation of a 1*c* TSD during epitaxy. The topography appearance reflects the sign of the Frank partials. Formation of carrot defects and threading dislocation clusters are also discussed. We found a smaller density of carrot defects in the (000-1) epilayers compared with that in the (0001) epilayers.

References

[1] S. Ha, P. Mieszkowski, M. Skowronski and L.B. Rowland: J. Cryst. Growth Vol. 244 (2002), p. 257

[2] S. Ha, H.J. Chung, N.T. Nuhfer and M. Skowronski: J. Cryst. Growth Vol. 262 (2004) p. 130

[3] M. Benamara, X. Zhang, M. Skowronski, P. Ruterana, G. Nouet, J.J. Sumakeris, M.J. Paisley and M.J. O'Loughlin: Appl. Phys. Lett. Vol. 86 (2005) p. 021905

[4] H. Chen, G. Wang, Y. Chen, X. Jia, J. Bai and M. Dudley: Mater. Res. Soc. Symp. Proc. Vol. 911 (2006), p. 163

[5] S. Izumi, H. Tsuchida, I. Kamata and T. Tawara: Appl. Phys. Lett. Vol. 86 (2005), p. 202108

[6] H. Tsuchida, I. Kamata and M. Nagano: J. Cryst. Growth vol. 306 (2007), p. 254

[7] H. Tsuchida, I. Kamata, T. Jikimoto and K. Izumi: J. Cryst. Growth Vol. 237-239 (2002), p. 120